

## Effects of tip geometry on interfacial contact forces

This article has been downloaded from IOPscience. Please scroll down to see the full text article.

2010 Modelling Simul. Mater. Sci. Eng. 18 034002

(<http://iopscience.iop.org/0965-0393/18/3/034002>)

[The Table of Contents](#) and [more related content](#) is available

Download details:

IP Address: 131.122.202.18

The article was downloaded on 05/03/2010 at 15:52

Please note that [terms and conditions apply](#).

# Effects of tip geometry on interfacial contact forces

M Todd Knippenberg<sup>1</sup>, Paul T Mikulski<sup>2</sup> and Judith A Harrison<sup>1</sup>

<sup>1</sup> Department of Chemistry, United States Naval Academy, Annapolis, MD, USA

<sup>2</sup> Department of Physics, United States Naval Academy, Annapolis, MD, USA

Received 7 October 2009, in final form 7 January 2010

Published 1 March 2010

Online at [stacks.iop.org/MSMSE/18/034002](http://stacks.iop.org/MSMSE/18/034002)

## Abstract

Experimental techniques that utilize atomic force microscopy are routinely used to examine tribological properties of tip–sample interactions. While analysis of data obtained with these methods provides values for macroscale properties, such as interfacial shear strength, understanding nanoscale properties, such as contact radius, requires an atomic-scale approach. Molecular dynamics simulations provide the ability to numerically analyze the nanoscale origins of a wide-range of material and tribological properties. In this paper, the sliding contact between a self-assembled monolayer (SAM) and two countersurfaces (a nominally flat, amorphous carbon surface and a nearly spherical fullerene tip) is compared. By examining contact forces between the tip and monolayer atoms, large differences in monolayer behavior that occur due to tip geometry can be elucidated. The structure factor reveals that the fullerene tip creates a more disordered monolayer than the amorphous counterface. Friction forces were also studied using the atomic-level contact forces, which show that the depth at which the fullerene tip affects the SAMs substrate is much deeper than the amorphous counterface. The distribution of contact forces that contribute to friction and load were studied and show a difference in behavior between the two countersurfaces. Finally, while there are a large number of atoms that have a non-zero load during sliding, a smaller subset of 32 atoms carries ~96% of the load. Using this subset of atoms to compute contact radius reveals a greater agreement with the continuum mechanics models than using all atoms with a non-zero load. This paper highlights how computer simulations can yield insight into tribological interactions at the atomic scale.

(Some figures in this article are in colour only in the electronic version)

## 1. Introduction

The behavior of materials at the nanoscale has been the subject of much recent interest [1–3]. This is largely due to the desire to make smaller machines, e.g. microelectromechanical systems (MEMSs) [4–6]. As the size of mechanical systems shrinks from macro- to nanoscale, the surface-to-volume ratio increases and surface phenomena, such as adhesion, friction and wear

become more significant. MEMSs are typically constructed of silicon because silicon etching technology is well developed. Silicon has a high surface energy and poor wear resistance. As a result, Si-based devices suffer from stiction (or adhesion) and severe wear in sliding contacts [7–12]. One way to lower surface energy, and thereby reduce stiction, is to coat the surface of Si-based MEMS with a solid lubricant, such as a self-assembled monolayer (SAM) or diamond-like carbon (DLC) [3, 6, 13–16]. Because SAMs form well-packed monolayers, they provide a flexible, convenient and simple system with which to tailor the interfacial properties of metals, metal oxides and semiconductors [17, 18].

The atomic force microscope (AFM) has proven to be a useful tool for examining mechanical properties and nanoscale tribology at well-defined interfaces [3, 19] and it has been used extensively to examine the mechanical and tribological properties of SAMs [20–36]. While the extraction of materials properties, such as Young's modulus and the interfacial shear strength, from AFM data requires the use of contact mechanics models [37, 38], recent simulations have cast doubt on the validity of these models at the atomic scale [39–42]. Robbins and coworkers [39, 40] examined the applicability of continuum mechanics to nanoscale contacts by comparing analytic continuum solutions to molecular dynamics (MD) simulations. These studies showed that atomic-scale roughness, due to the presence of discrete atoms, leads to dramatic deviations from analytical continuum solutions during indentation. During sliding, contact areas and stresses can be changed by a factor of two compared with analytic continuum solutions. Recently, complementary MD and hierarchical finite-element-MD simulations were used to examine contact area as a function of roughness in model diamond nanocomposites (MDN) [42]. The roughness was varied by randomly tilting the embedded diamond grains within the nanocomposites. Configurations created for the MD simulations served as templates for the finite-element (FE) mesh. In both the MD and FE simulations, the additional component of roughness from the tilting of the diamond grains increased the contact area compared with the analytic continuum solution. Contact areas of the MDN calculated in the MD simulations were larger than systems that are atomically flat which possess roughness associated with the presence of discrete atoms [41]. In addition, while the inclusion of tilted diamond grains in the FE simulations increased the contact area compared with the continuum solutions, the increase was not as large as it was in the set of complementary MD simulations. Despite the fact that continuum contact models underestimate the contact area, they have been successfully used to interpret AFM data [3, 19, 37, 41, 43–51]. This apparent contradiction has yet to be fully understood.

The addition of a compliant layer, such as a SAM, to a substrate adds an additional level of complication. Recently, several contact models for the case of a thin, compliant layer attached to a substrate have appeared in the literature. For instance, Johnson and Sridhar [52] extended Johnson–Kendall–Roberts (JKR) theory to include a compliant elastic coating on a compliant substrate. Viscoelastic effects have been incorporated into JKR theory so that the modulus of elastomeric films could be studied [53]. Lin *et al* modeled the compliant layer as a Neo–Hookean layer [54]. Finally, Reedy [55] developed a model for the contact of a rigid, spherical indenter contacting a thin, linear elastic coating to a rigid substrate. Despite the existence of these models, there are only a few cases of their successful application to the AFM data of deformable materials [56–58].

MD simulations have proven to be a useful tool for lending insight into atomic-scale processes. Since the ground-breaking MD simulations of the indentation of Au(1 1 1) [59] and a two-dimensional Lennard-Jones crystal [60], MD simulations have been used extensively to model nanoindentation [61–70] and friction [71–77]. Despite the successes in modeling indentation and the friction between two infinitely flat surfaces, there have been comparatively few MD studies that have examined friction using finite-size tips [39, 40, 42, 64, 70, 75, 78–80].

In this work, MD simulations were used to examine contact behavior and atomic-scale friction obtained when countersurfaces with two different geometries are brought into contact and slid against model SAMs composed of *n*-alkane chains on a hard substrate. Careful examination of the contact forces on each monolayer atom, or the vector sum of forces exerted on each atom due to interactions with the entire set of countersurface atoms, provides unprecedented insight into the contact behavior and the friction [70, 81–83]. The way in which individual monolayer atoms support load and contribute to friction in both contacting geometries was examined. The results presented here, combined with previous simulations that have examined the validity of continuum mechanics models at the nanometer scale [39–42, 70], may prove helpful in the application, and development, of contact mechanics to systems with compliant layers.

## 2. Simulation details

All simulations discussed herein employ the adaptive intermolecular reactive empirical bond-order (AIREBO) potential [84], which takes into account each atom's local environment, torsional interactions between atoms, and non-bonded interactions. This hydrocarbon potential has been used extensively in a variety of tribology simulations [64, 77, 81]. Additionally, this potential has been used in chemical sputtering of polymers [85], hydrocarbon sputtering [86, 87], and carbon nanotube bending [88], and chemistry [89–91]. The AIREBO potential also can simulate chemical reactions, which may occur if forces are large enough to break bonds during sliding [67, 74, 92].

To examine the effects of contact geometry on indentation and friction, two different countersurfaces were placed in sliding contact with a model SAM composed of *n*-alkane chains containing 14 carbon atoms ( $-(\text{CH}_2)_{13}-\text{CH}_3$ ) attached to a diamond (1 1 1) surface in the  $(2 \times 2)$  arrangement. (The alkane chains will be referred to as  $\text{C}_{14}$  chains.) The result is a monolayer surface area of  $21.9 \text{ \AA}^2$  between hydrocarbon chains and a packing density that is similar to that of *n*-alkanethiols on Au(1 1 1) [93]. The terminal  $-\text{CH}_2$  group in the chains is chemically bound to the diamond (1 1 1) substrate (this last  $-\text{CH}_2$  group contains the head carbon). The diamond substrate contains three layers of carbon atoms, with the bottom (outermost) layer of carbon held rigid. The remaining two layers of diamond have a Berendsen thermostat applied to them and are maintained at 290 K [94]. The positions of the  $\text{C}_{14}$  chains within the monolayer are integrated without constraints during the course of the simulation.

Both an infinitely flat amorphous carbon counterface and a spherical fullerene tip were placed in sliding contact with the model SAMs. The amorphous carbon surface has been used previously [81] and is described briefly below. It consists of 5500 atoms, of which 35% are hydrogen (figure 1). It has a density of  $2.3 \text{ g cm}^{-3}$  and the surface in contact with the monolayer is fully saturated with hydrogen at the start of the simulation. The total thickness of the amorphous counterface is approximately  $19.3 \text{ \AA}$ . The counterface length and width are such that it has the same dimensions as the monolayer beneath it. Periodic boundary conditions are applied in the plane containing the monolayer and, as a result, both the monolayer and the amorphous counterface are infinite in extent. The number of  $\text{C}_{14}$  chains that are attached to the diamond substrate is based on the size of the sliding countersurface. The simulations involving the amorphous counterface have 100 monolayer chains, while the fullerene tip is in sliding contact with a monolayer composed of 270 chains. The *x* and *y* dimensions of the simulation system when the amorphous counterface and fullerene tip are used are  $50.3 \text{ \AA}$  by  $43.6 \text{ \AA}$  and  $75.4 \text{ \AA}$  by  $78.4 \text{ \AA}$ , respectively.

The amorphous counterface is partitioned into three distinct regions. The atoms in the upper  $5 \text{ \AA}$  of the counterface are held rigid (figure 1). Moving inward toward the interface,

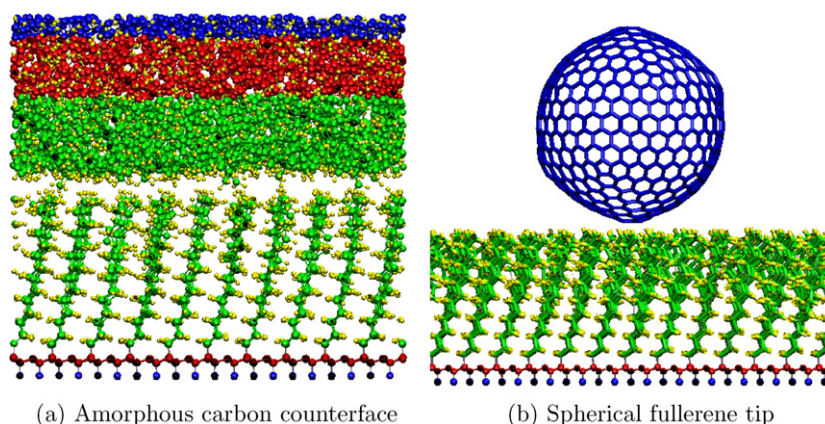


**Figure 1.** Simulation snapshots for the infinitely flat amorphous counterface and the finite-sized spherical tip under an applied load of 0 nN. In both snapshots, atoms colored blue, red, and green are held rigid, have a thermostat applied to them, and are integrated in time without constraints, respectively. Hydrogen atoms in the tip and in the monolayer are colored yellow. The sliding is along the chain cant or from left to right. (Some atoms in the diamond substrate are not shown for clarity.) (a) Amorphous carbon counterface and (b) Spherical fullerene tip.

the atoms in the next 6.5 Å are thermostated to 290 K, and the atoms in the remaining 7 Å closest to the interface between counterface and substrate are integrated without constraints. A constant velocity of  $0.8711 \text{ Å ps}^{-1}$  is applied in the sliding direction to the rigid layers of the counterface, which corresponds to moving one unit cell of the  $(2 \times 2)$  diamond substrate every 10 ps. While the sliding speed is much faster than experimental sliding speeds, simulated results have been shown to be invariant for sliding speeds ranging from 0.2 to  $100 \text{ m s}^{-1}$  in several systems [95–97].

To mimic an AFM study, a finite-size rigid spherical tip is also placed in sliding contact with a model SAM. The spherical tip is composed of 720 carbon atoms, had a radius of  $\sim 13 \text{ Å}$ , and was composed entirely of 5-membered or 6-membered rings so that its shape resembled that of a 720-atom fullerene (figure 1) [98]. The tip is held rigid while sliding across the monolayer substrate to mimic a hard AFM probe interacting with the much softer alkane monolayer (figure 1).

The counterfaces and monolayers are equilibrated separately. Equilibration is achieved when both the potential energy and the temperature of the system fluctuates about some constant value. Once equilibration was achieved, both countersurfaces were introduced above the monolayer and the systems were equilibrated with a target load applied to the countersurfaces during sliding. During the course of this equilibration, the counterface can move closer to, or away from, the monolayer through the use of a feedback loop which computes the forces between counterface atoms and the monolayer atoms, [81, 82] raising or lowering each counterface to arrive at the target load. Equilibrating the countersurface and monolayer substrate together for two complete passes over the surface reduces the effect of run-in in the simulations. Once the equilibration is complete, then sliding data are collected for a total of two passes, which corresponds to 18 unit cells of the monolayer substrate (or the unit cell of the underlying  $(2 \times 2)$  diamond substrate).

The average atomic contact force is defined as the force on an individual monolayer atom due to all counterface atoms averaged over  $N$  time steps and is calculated using the following

equation [70, 81–83]:

$$F = \frac{1}{N} \sum_i^N \left( \sum_j^{\text{monolayer}} \sum_k^{\text{counterface}} F_{jk} \right). \quad (1)$$

Here,  $i$  is the sum over a set of a user-specified set of simulation steps ( $N$ ),  $j$  is the sum over the entire number of atoms in the monolayer,  $k$  is a single counterface atom, and finally  $F_{jk}$  is the instantaneous force between atoms  $j$  and  $k$ .

It is important to note that the quantity that is most directly connected with what is measured experimentally is the *net* force on the rigid-layer counterface atoms, not the average atomic contact force summed over all counterface atoms (i.e. the net average contact force). In fact, the atomic contact forces on rigid-counterface atoms and atoms near the rigid layer are completely negligible because they are far away from the sliding interface. It has been recently shown that over the course of a simulation, there is a high degree of correlation between the *net* force on rigid-layer counterface atoms and the *net* average contact force exerted by the sample on the counterface [99]. These average contact forces can be analyzed in creative ways to yield insight into the way in which structural features at the sliding interface influence friction force [82, 83, 99]. The main advantage of using the average atomic contact forces is that the forces on individual monolayer (or counterface) atoms normal to, and tangential to, the sliding interface, and the role they play in supporting the load and friction, can be investigated. In particular, the contributions each atom makes to the total force that resists the forward motion of the counterface can be separated from the contributions that push the counterface in the sliding direction. Loading forces on each monolayer atom can also be separated into repulsive and attractive contributions. For simplicity, hereafter, contact force will refer to the average atomic contact force on each monolayer atom.

### 3. Results

The major difference between the amorphous counterface and the spherical fullerene tip is that the spherical tip is able to penetrate into the monolayer, while the amorphous counterface uniformly compresses the monolayer. This fact leads to markedly different behavior when comparing the two countersurfaces. For example, a comparison of the average contact friction calculated over the duration of the sliding simulations (two complete passes) as a function of applied load using both counterfaces is shown in figure 2. At non-zero loads, the friction calculated using the fullerene tip is larger than the friction produced from the amorphous counterface. In addition, when the spherical fullerene tip is used, the magnitude of friction increases approximately linearly with load and it increases much more rapidly with load compared to the friction generated by the amorphous counterface. When the amorphous counterface is used, the friction reaches some limiting value as the load increases. Because the amorphous system is composed of a counterface and substrate that have the same dimensions as the sliding interface, there is not any ‘edge effect’ like that seen when the fullerene tip is sliding. As a result, the amorphous counterface is not able to penetrate into the substrate.

Both experiments [23, 24, 29, 31] and simulations [77, 81, 82, 100] have linked increased friction to an increase in disorder. Calculation of the two-dimensional (2D) structure factor,  $S_2$ , and the number of gauche defects in the monolayer, are two possible ways disorder within the monolayer can be quantified. The 2D structure factor has been defined previously [64, 99]. Treating the  $-\text{CH}_2-$  and  $-\text{CH}_3-$  chain segments as layers within the monolayer allows the structure factor to be calculated as a function of chain segment. Perfectly ordered chains would be translationally invariant and have structure factors of one. As chains become

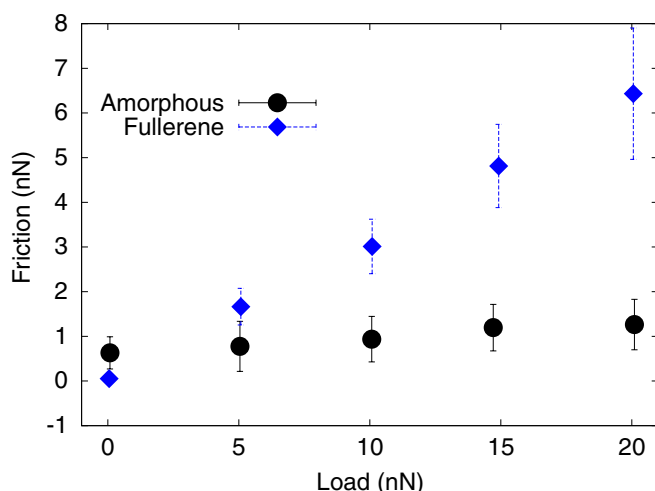


**Figure 2.** Average contact friction as a function of load when both countersurfaces are in sliding contact with a monolayer composed of  $C_{14}$  alkane chains. The values represented by the points are obtained by averaging the friction (computed with equation (1) and  $N = 2000$ ) as a function of time at a given load. The error bars represent one standard deviation.

more disordered, the value of  $S_2$  moves toward zero, indicating the monolayer's ordering has changed. Because the  $C_{14}$  chains within the monolayer are anchored to a (1 1 1) diamond substrate in a  $(2 \times 2)$  arrangement,  $S_2$  may be calculated using the reciprocal lattice vectors of the reconstructed diamond surface.

The structure factors calculated for each carbon atom in the monolayer are shown in figure 3 for both countersurfaces. At a given load, the structure factor of each carbon atom in the monolayer is averaged over the entire sliding simulation. Each carbon atom in the monolayer chain is numbered from 1 to 14, with 1 being the head carbon atom, and 14 being the  $-CH_3$  group closest to the sliding interface. For both countersurfaces, the farther the chains extend from the substrate toward the sliding interface, the more the packing deviates from that of the underlying diamond substrate. In the case of the fullerene tip, the ends of the chain's closest to the sliding interface lose all the order associated with the underlying diamond substrate. That is, the structure factors approach zero even at the lowest load of 0 nN. Increasing the load on the fullerene tip results in an increase in disorder. In contrast, when the amorphous counterface is used, the application of load results in more order. Put another way, the structure factors become more tightly correlated with the underlying diamond substrate. This increase in order as a function of load is a result of the tighter packing brought about by the compression, and the aligning of the  $-CH_3$  tail groups at the higher loads. This also results in a uniform response of the monolayer to the motion of the counterface [77, 101, 102].

The formation of gauche defects has been noted in previous MD simulations of indentation [64, 77, 82, 103], and has also been suggested to lead to higher interfacial friction [20, 23]. A gauche defect can be defined as the occurrence of a dihedral angle,  $\phi$ , in the monolayer chain, that is larger than  $270^\circ$  or lower than  $90^\circ$  between four consecutive carbon atoms  $C_1-C_2-C_3-C_4$  when looking down the  $C_2-C_3$  bond. In simulations by Tutein *et al* as the load of a rigid nanotube was increased during indentation of a SAM, the number of gauche defects increased [64]. In those simulations, the gauche defects were computed while a (10,10) single-walled carbon nanotube (SWNT) was used to indent monolayers composed of chains with different lengths.

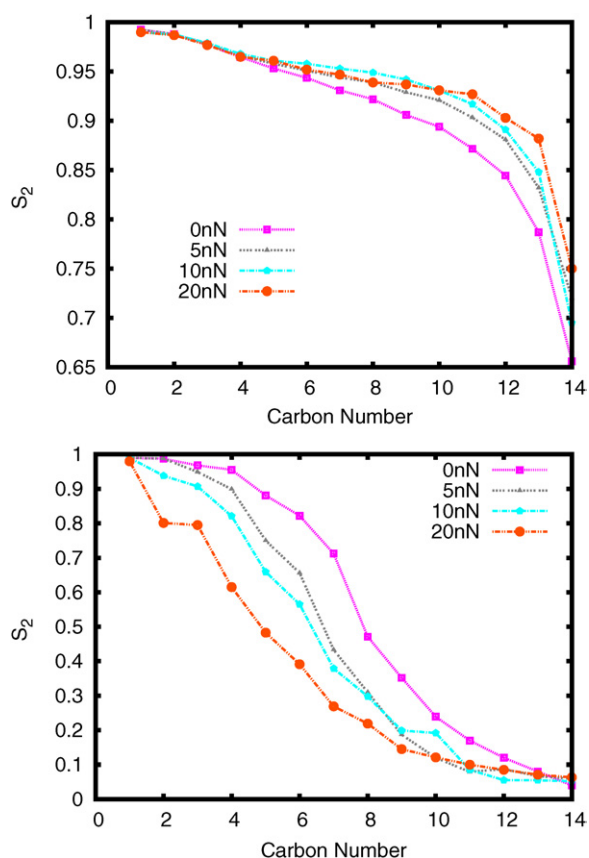


**Figure 3.** Two-dimensional structure factors for both monolayers in sliding contact with the amorphous counterface (top) and fullerene tip (bottom). Each carbon atom is numbered 1–14, with 1 corresponding to the head carbon atom. Carbon numbered as 14 is the carbon atom closest to the sliding contact or the tail group.

Figure 4 shows the plot of the total number of gauche defects in the monolayers when in sliding contact with both countersurfaces at a fixed load. Each set of four consecutive carbon atoms in a chain is examined to determine the dihedral angle, meaning that the entire monolayer is being examined for gauche defects. At all loads examined, the fullerene tip generates a larger number of gauche defects during sliding. In fact, the fullerene tip generates approximately ten times the number of gauche defects at all non-zero loads by the end of the second pass of the tip through the monolayer.

When the amorphous counterface is used, penetration into the monolayer is not possible. As a result, the number of gauche defects decreases slightly as sliding progresses, before eventually plateauing. In this case, the gauche defects are localized to the ends of the chain and the sliding motion has the net effect of removing the defects from the ends of the chains. In the case of the fullerene tip, the number of gauche defects is approximately constant during the course of the simulation. Gauche defects can be formed far below the sliding interface (figure 4) because the fullerene can penetrate into the monolayer. The number of defects is approximately constant because new defects are being formed in the region around the tip while defects far from the tip eventually anneal out.

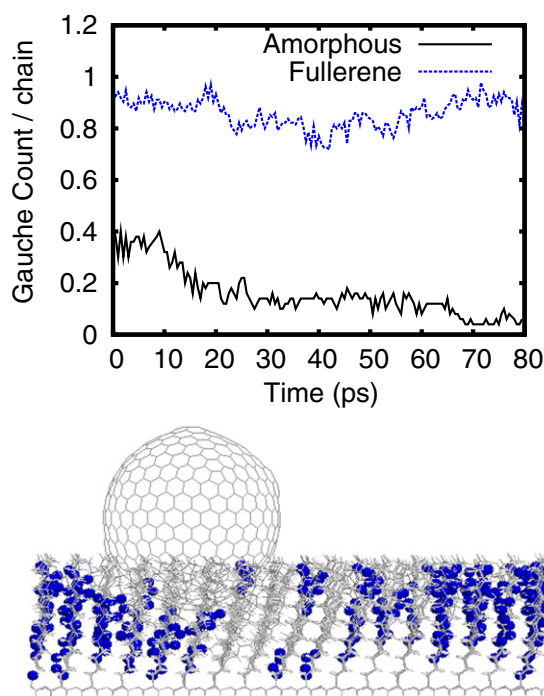


**Figure 4.** (upper panel) Number of gauche defects per chain during sliding when the counterface is under a constant load of 10 nN. The gauche count is normalized for the number of  $C_{14}$  chains that are attached to the (1 1 1) diamond. It should also be noted that time zero corresponds to the end of the equilibration stage of the simulation. The counterface is in sliding contact with the monolayer during the equilibration phase. (lower panel) Simulation snapshot of the placement of gauche defects when the fullerene tip is in sliding contact with the monolayer under 10 nN of load. For clarity, the monolayer atoms which have a gauche defect are shown as blue spheres, while the remaining atoms in the system are shown in wireframe format.

From the average atomic contact forces on each monolayer atom calculated using equation (1), a detailed analysis of the way individual atoms contribute to the total friction is possible [70, 81, 82, 99]. Once contact forces are calculated, they can be analyzed in creative ways to lend insight into the distribution of forces at the sliding interface. For example, figure 5 shows the distribution of contact forces on all the monolayer atoms in the sliding direction as a function of position from the center of the fullerene tip. Positive distances correspond to monolayer atoms in front of the tip in the sliding direction. At this load, the contact forces directly in front of the tip are larger than those behind the tip.

These forces can be broken down even further by separating them into components that resist (+) tip motion and those that push (−) the tip in the sliding direction (figure 5). By breaking down the sliding-force distribution in this way four distinct regions become apparent. A region of resisting (+) and pushing (−) forces in front of the tip and regions of positive and negative forces behind the tip. Atoms in front of the tip (+y values) naturally oppose the motion of the tip moving past them. When these atoms are in close proximity to the tip, they interact via the hard-wall portion of the LJ potential. This hard-wall interaction gives rise to the (+) values of contact force in front of the tip (+y) (figure 5).

When the tip passes over, or by, the monolayer atoms, the tip and the monolayer interact via the hard-wall portion of the LJ potential; however, the sign of the force changes to (−).

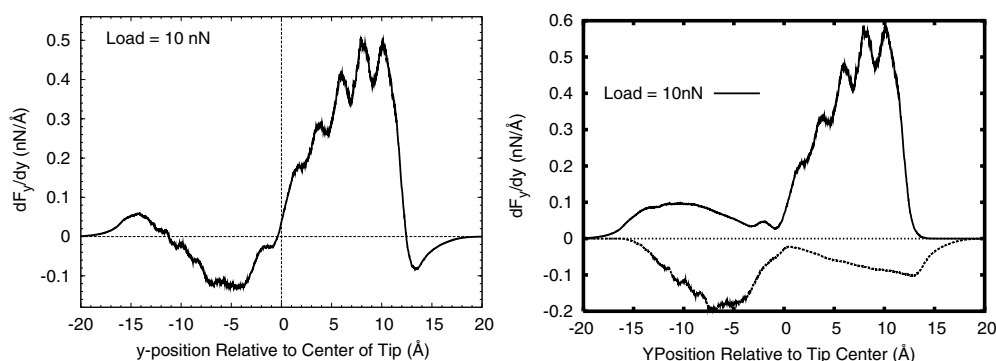


**Figure 5.** (left) The average *total* contact force in the sliding direction on all the monolayer atoms as a function of distance from a fixed atom at the bottom center of the fullerene tip. The friction in figure 2 can be obtained by integration of the area under this curve. (right) The same distribution of contact forces except that in this distribution resisting (+) and pushing (−) forces are traced (and binned) separately. The load on the fullerene is 10 nN in both panels.

As a result, atoms behind the tip (−*y* values) are able to exert a force on the tip in the sliding direction that aids the motion of the tip. These regions of (−) force behind the tip are apparent in distributions at 10 nN shown in figure 5 and at all other non-zero loads. Because this force is ‘pushing’ the tip in the sliding direction, it reduces the net friction force experienced by the tip. The scale of the forces in the two regions of the contact force distribution that arise from the hard-wall portion of the LJ potential is larger than the scale of the forces in the remaining two regions of the distributions. This disparity increases with the application of load. It follows that these types of interactions are the largest contributors to the net friction force experienced by the monolayer. It should also be noted that for all non-zero loads, there is a pronounced difference in the scale of the resisting forces (+) in front of the tip compared with the scale of pushing forces (−) behind the tip [70]. In summary, figure 5 can be broken down into four quadrants around the origin. The larger of the two quadrants behind the tip center are atoms that exert a negative force behind the sliding countersurface that ‘push’ the tip forward. The larger of the two quadrants in front of the tip center with positive forces are atoms in front of the tip that are being pushed closer to monolayer atoms, and therefore ‘feel’ the hard repulsive wall of the potential. These forces resist forward motion of the tip.

The remaining two regions of the sliding-force distribution (figure 5) correspond to the resisting forces (+) behind the tip (−*y*) and to the pushing forces (−) in front of the tip (+*y*). Both of these types of forces arise from long-range interactions. When the tip has passed by a monolayer atom, the distance between the monolayer atom and the tip increases so that the interaction is governed by the attractive region of the LJ. Because the force is attractive, the monolayer atom resists the motion of the tip moving away from it. These forces correspond to the resisting (+) forces at negative values of tip position (−*y*) in the distribution. There are monolayer atoms that are far enough in front of the tip to be in the attractive region of the potential. This attractive force ‘pulls’ the tip in the sliding direction and is, therefore, classified as a pushing force at positive values of tip position (+*y*). These two regions of the distribution are a direct consequence of the finite-size of tip and are not apparent in contact-force distributions when the infinite, amorphous carbon tip is in sliding contact with the monolayer (figure 6).

In contrast to the regions of the distributions that arise from interactions with the hard wall of the LJ, the regions that arise from attractive interactions involve large numbers of atoms.

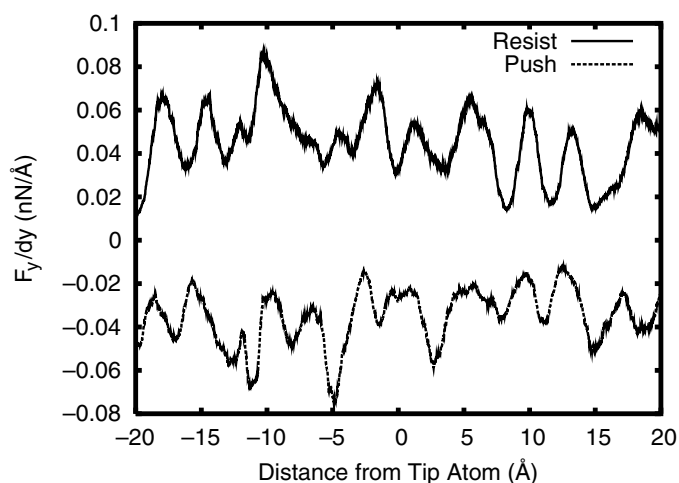


**Figure 6.** Average total contact friction on the monolayer atoms separated into components that resist (+) the amorphous counterface motion and those that push (−) the amorphous counterface along the sliding direction. The load on the amorphous carbon counterface is 10 nN. Because the amorphous counterface and the monolayer are infinite in extent, a random counterface atom is chosen to compare distance from counterface to subsequent monolayer chains.

Due to the long-range nature of the attractive portion of the LJ, more atoms contribute to these portions of the distributions. However, because the attractive portion of the LJ potential is weaker than the repulsive region, the scale of the forces in these two regions of the distributions is much smaller.

The amorphous counterface is infinite in extent and it cannot penetrate into the monolayer. As a result, the scale of the contact forces generated by the motion of the counterface is much smaller than when the fullerene tip is used (figure 6). The distribution of contact forces during sliding is periodic. Because the periodic boundary conditions of the amorphous counterface match the monolayer dimensions, a random atom is chosen, and distances between this counterface atom and substrate atoms are calculated. At all points along the monolayer there are some resisting and pushing forces on the counterface. Similar behavior is seen at all applied loads, indicating that the monolayer structure beneath the sliding counterface does not change drastically during the course of sliding or with the application of load. The magnitude of the forces are larger, but the overall behavior is the same at all loads.

The contact force on each monolayer atom due to all countersurface atoms can be collected so that the contact forces on specific segments, or groups, of atoms within the monolayer chains can be calculated. Figure 7 shows the contact forces in the sliding direction (friction) grouped by chain segment when the amorphous counterface is in sliding contact with the monolayer. At 0 nN, the contact forces of the tail groups of each chain (−CH<sub>3</sub>) are plotted together and labeled group 14. Moving down the chain toward the attachment point on the substrate, the group numbers are decremented by one for each group. Thus, group number one would correspond to the head groups attached to the diamond substrate. It is clear that the tail groups of the chains have the largest forces that resist (+y) countersurface motion and the largest forces that assist countersurface motion (−y). The farther the chain segment is away from the sliding interface, the smaller the magnitude of the contact forces (figure 7) on that group of atoms. In fact, only the top three groups have any appreciable contact forces at a load of 0 nN.

It is also possible to subdivide the contact forces on the groups further, separating them into individual atomic contributions. In that case, previous simulations have shown that two of

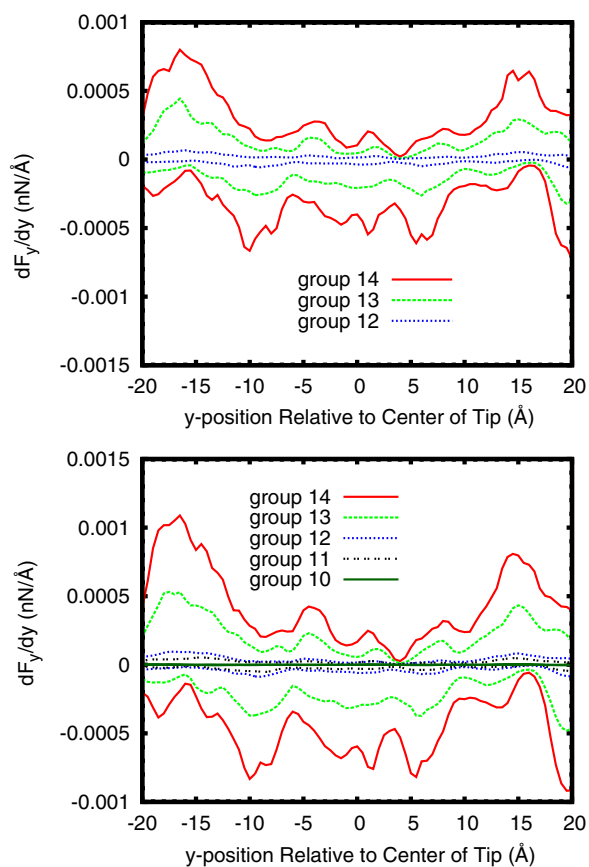


**Figure 7.** Average total contact friction on groups of monolayer atoms (chain segments) separated into components that resist (+) the counterface motion and those that push (–) the counterface and the sliding direction. The load on the amorphous counterface is 0 nN (top) and 10 nN (bottom).

the three hydrogen atoms in the tail groups protrude upward toward the amorphous counterface and are responsible for the majority of the friction in a monolayer composed of  $C_{14}$  alkane chains [82]. As the magnitude of the applied load increases, the amount of friction generated by each portion of the monolayer increases slightly and additional groups, farther down the chains, begin to have non-negligible contact forces. However, the tail groups continue to contribute the bulk of the contact forces to the overall friction.

Examination of the contact forces in the sliding direction based on the position within the monolayer chain when the fullerene tip is used reveals a much different picture. Figure 8 shows the evolution of contact force on individual chain segments as a function of load. At an applied load of 0 nN, the highest friction-generating group of the monolayer is the tail ( $-CH_3$ ) group. At this load, the fullerene has not penetrated the monolayer (figure 1). As a result, groups 14 and 13 have modest frictional forces and the rest of the chain segments within the monolayer contribute essentially nothing to friction. As the applied load increases, the fullerene begins to penetrate into the monolayer (figure 10). For all non-zero loads, the bottom of the tip is now found below the tail  $-CH_3$  group and interacts with more of the monolayer chain than it did at 0 nN. As a result, friction is generated from more than the top two groups in the monolayer. Additionally, there is a shift in which chain segments generate the most friction. At both 10 nN

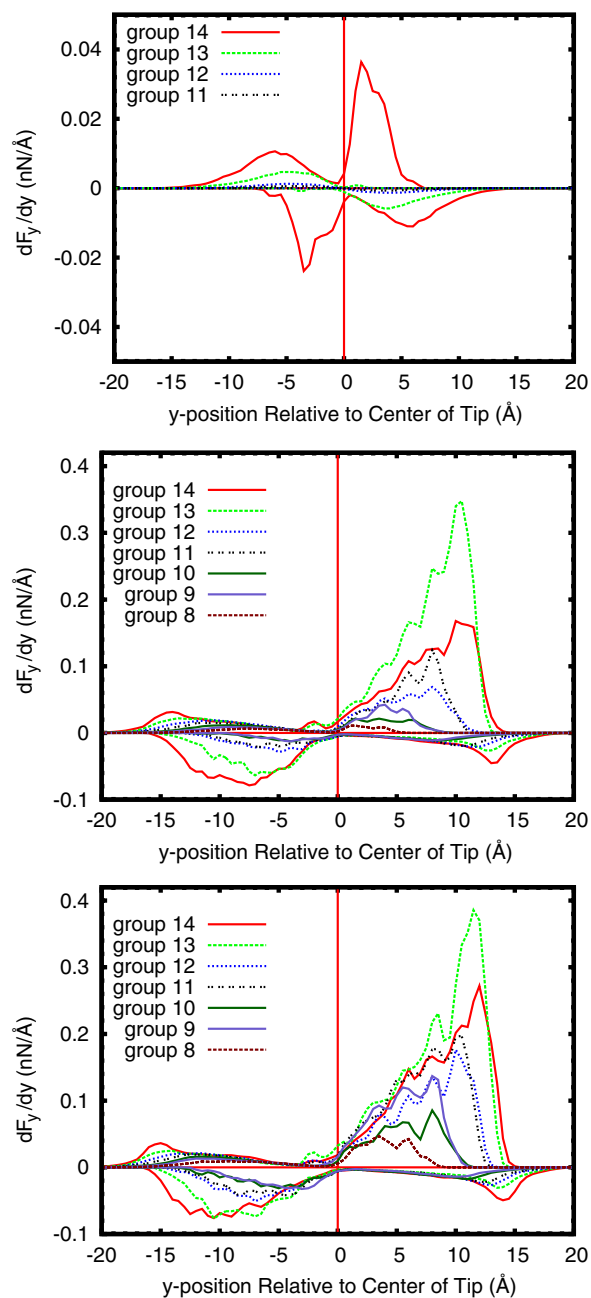


**Figure 8.** Average total contact friction on groups of monolayer atoms (chain segments) separated into components that resist the tip motion and those that push the tip and the sliding direction. The load on the fullerene tip is 0 nN (top), 10 nN (middle) and 20 nN (bottom).

and 20 nN (figure 8), the highest friction-generating group is the group directly beneath the tail group. In fact, a pattern emerges that the odd-numbered chain segments, due to the zig-zag geometry of the  $n$ -alkane chains, have a higher friction than the even-numbered groups directly above them. This behavior is seen in all groups moving down the chain from the tail toward

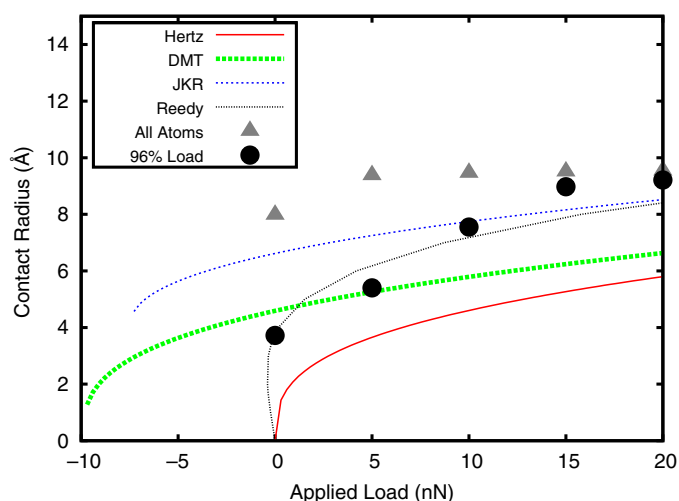


**Figure 9.** Simulated and calculated contact radii as a function of load when the fullerene tip is brought into contact with the monolayer.

the attachment point to the diamond. The tail group has the ability to move farther away from the tip. However, chain groups farther down the chain are restricted by the close proximity of the neighboring monolayer chains. The sliding direction is the direction of the chain *cant*, and the odd-numbered groups are closer to the fullerene tip when it has penetrated the monolayer.

The contact area can be easily calculated when the amorphous counterface is used because it is infinite in the plane containing the monolayer. Thus, the contact area is taken to be the same as the simulation cell dimensions. In contrast, calculating the contact area when a finite-size tip is used is subject to some uncertainties. In MD simulations, as in experiment, contact between the tip and the monolayer must be defined. Chandross *et al* defined contact to be the point where the distance between the tip and monolayer was smaller than 0.5 nm [79]. This definition was used to exclude some atoms from contact due to the long-range coulombic terms in the potential. In the simulations performed here, the contact force on each monolayer atom due to the tip is computed; thus, the contact area could be defined as the number of monolayer atoms with non-zero force in the loading direction divided by the total number of surface atoms times the area of the computational cell. Previous MD simulations have also used this definition to calculate contact area [39–42, 70]. Because the fullerene tip is spherical, contact areas are approximately circular and can be converted into contact radii.

The simulated values for the total contact radius as a function of load, as well as the calculated contact radius using the Hertz [104], Derjaguin–Muller–Toporov (DMT) [105], JKR [106], and contact areas obtained using the thin-coating contact mechanics (TCCM [55]) model with adhesion forces for JKR-like behavior are also shown in figure 9. These contact mechanics models require values for the work of adhesion,  $\gamma$  and a Young's modulus and Poisson ratio for both the tip and the substrate. The value  $121 \text{ mJ m}^{-2}$  for  $\gamma$  was calculated by integrating the force curve generated by bringing the fullerene tip into contact with the SAM and dividing by the contact area when the force transitions from attractive to repulsive ( $F = 0$ ). This procedure has been used successfully to determine the work of adhesion for diamond and diamond-like carbon self-mated contacts [107]. This calculated value of  $\gamma$  is in reasonable agreement with  $\gamma$  values for  $\text{C}_{12}$  ( $104.1 \text{ mJ m}^{-2}$ ) and  $\text{C}_{18}$  ( $82.8 \text{ mJ m}^{-2}$ ) alkanethiols

on gold [108]. Experimentally determined values of elastic modulus of monolayer films vary widely with reported values ranging from 0.18 to 75 GPa [108–112] with some studies suggesting the value is independent of chain length [110] and other studies suggesting the opposite [113]. Young's modulus of thin films is difficult to measure and can be influenced by the substrate. DelRio *et al* used the AFM and near edge x-ray absorption fine structure spectroscopy to determine the work of adhesion, Young's modulus and the dichroic ratio of alkanethiols on gold. The value of Young's modulus and the order within the monolayer decreases slightly with decreasing chain length [108]. Because the monolayers used here are perfectly ordered, the modulus for C<sub>18</sub> chains (1.00 GPa) is used to calculate the data in figure 9. (It should be noted, however, that the contact radius calculated using contact mechanics models is sensitive to the choice of Young's modulus.) For Poisson's ratio of the monolayer, we adopt the value of 0.4 for a compliant 10 Å thick coating attached on a rigid substrate reported by Reedy [55].

It is clear from figure 9 that the contact radius computed using all the monolayer atoms with a non-zero contact force in the simulations is much larger than the area predicted by the Hertz, DMT, or the JKR models. This is not surprising given the fact that these models do not take into account the compliant monolayer, these models assume perfectly flat surfaces, and that the chemical potential used for the simulations includes long-range interactions through the Lennard-Jones potential. The TCCM model includes an adhesive force and takes into account the presence of a compliant layer and does a reasonable job predicting the contact radius at high loads. However, the contact radius decreases too quickly with decreasing load compared with the simulations.

Previous simulations have shown that a small number of atoms in the contact are responsible for carrying the majority of the load and friction when a fullerene tip indents a monolayer [70]. Over the course of the entire sliding simulation, on average there are 32 atoms (figure 10) with non-zero force in the loading direction that are responsible for ~96% of the load. The contact radii calculated using the 32 atoms that support the majority of the load (at that point during the sliding) are also shown in figure 9. (It should be noted that during sliding the identity of 32 atoms with the largest contact forces changes. Despite this, there are always 32 atoms that support ~96%.) Using this definition, the contact radii as a function of load closely resemble that obtained using the TCCM model. It should be noted, however, there is some disparity between the simulations and the optimal conditions for which the Reedy model was developed. Specifically, the Reedy model supposes that the radius of the indenter is much larger than the height of the substrate the indenter is in contact with ( $R \gg h$ ). In the case of these simulations, the height of the monolayer is slightly larger than the tip radius. Also, the calculated contact radius is assumed to be much greater than the height of the monolayer ( $a \gg h$ ). At low loads, this is not the case for these simulations, and even at the highest load, the calculated contact area is only slightly larger than the height of the substrate. Despite these differences, the TCCM model with adhesion added provides the closest fit for the contact radii computed using the 32 atoms that support ~96% of the load (figure 9).

#### 4. Conclusion

In this paper, simulations were performed by placing both an amorphous carbon counterface and a spherical fullerene tip in sliding contact with SAMs composed of *n*-alkane chains with the chemical formula –C<sub>14</sub>H<sub>29</sub> attached to diamond (1 1 1). Due to the differences in the geometry of the countersurfaces, the amorphous carbon counterface was able to distribute the applied normal load onto all monolayer chains, while the finite-size fullerene tip had a localized affect on the monolayer chains beneath it and in close proximity to it.

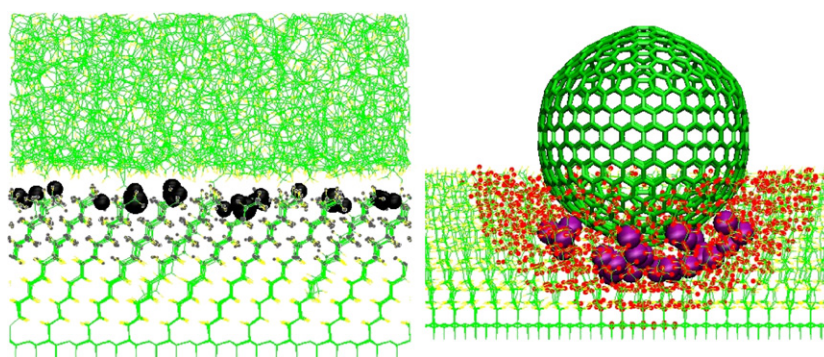


**Figure 10.** The simulated systems viewed from the side in wireframe format. The 32 atoms with the largest repelling forces are represented by big spheres. (These atoms carry  $\sim 96\%$  of the load.) Small dots represent all atoms with non-zero values of contact force in the loading direction. (left panel) The amorphous counterface system under a 20 nN. (right panel) The fullerene tip system under a 10 nN load.

Single asperity contact measurements, such as those obtained with an AFM, have proven to be a very useful tool for examining mechanical and tribological properties at well-defined interfaces. Measurements made with the same tip on different substrates yield *qualitative* information about mechanical and tribological properties of the contacting pairs. For instance, there have been many examinations of the friction of SAMs as a function of chain length [31, 34, 114], terminal-group identity [25, 26, 28, 114, 115], and packing density [23, 29]. Taken together, these measurements point to a link between friction and interfacial order, with friction increasing as the amount of the order decreases. MD simulations of SAMs have revealed similar trends [77, 81, 82, 99–101, 103]. In contrast to the experiments, the nature of simulations allows for specific structural features at the interface to be linked to the calculated friction.

In the work presented here, finite-size tips were shown to induce significant disorder within the monolayer compared with amorphous (nominally flat) counterfaces. The amount of disorder was monitored by calculating the two-dimensional structure factor and the number of gauche defects within the monolayer chains. These defects are distributed throughout the chains. In the case of the finite-size tip, increasing the load increases the number of gauche defects within the chains and increases disorder within the monolayer. In contrast, the amorphous carbon countersurface introduces gauche defects that are largely localized at the ends of the chains. This has also been observed in monolayers composed of shorter and longer chains [103]. In addition, because the main effect of increasing the load is compression of the monolayer, the application of load causes the chains to be more uniformly packed, increasing the order of the monolayer. Clearly, this effect relies on the complex interplay between contact area and packing density. In other words, penetration of the countersurface into the monolayer, or increased spacing between chains within the monolayer, will disrupt this effect.

By calculating the contact forces at the interface between the countersurfaces and the monolayer, atoms that carry the majority of the load, or are responsible for the majority of the friction, were identified. The simulations show that with the amorphous carbon counterface the load and the friction are distributed over the entire surface of the monolayer and the largest forces are localized to the tail groups within the chains. Examining these contact forces atom by atom has shown that it is the hydrogen atoms within these groups that carry the bulk of the repulsive and the resisting forces while the carbon atoms have mostly attractive and pushing

forces [82]. When the countersurface becomes finite-sized, the way in which load and friction are distributed within the monolayer changes dramatically. At all non-zero loads, the load and the friction are localized around the tip. While a large number of atoms within the chains contribute to the total load in the total friction, the simulations show that a small number of atoms are responsible for carrying the bulk of the load and the friction. The orientation of the chains and the direction of the sliding cause the odd-numbered chain segments ( $-\text{CH}_2-$  or  $-\text{CH}_3$ ) to have higher contact forces than the even-numbered chain segments.

To obtain *quantitative* information from AFM measurements, details regarding the shape of the contact, such as the shape of the counterface, and mechanical properties of the contacting materials must be known. Once these details are known continuum contact models have been routinely used to extract properties, such as Young's modulus and interfacial shear strength from the AFM data. Recent MD simulations have shown that continuum contact models underestimate the contact area of nanoscale contacts. Despite the fact recent MD simulations show that continuum contact models underestimate the contact area [39–42], they have been successfully used to interpret AFM data [3, 19, 37, 41, 43–51]. The addition of a compliant layer on the substrate complicates the analysis of the AFM data.

The results presented here may provide an insight into the apparent contradiction discussed above. Herein, when a finite-size tip is used it is shown that the majority of the load and friction arises from interactions of the tip with a small number of atoms, while many more atoms contribute to the total load and total friction. There are 1321 atoms that have non-zero contact forces in the loading direction while only 32 atoms contribute to the majority of the load ( $\sim 96\%$ ). If this subset of atoms is used to calculate the contact radius as a function of load, the results match very well with the recently developed contact model for a compliant layer on a hard substrate [55]. The fact that the interaction of a few atoms is responsible for the bulk of the load and the friction is important if one considers an AFM tip. Even if the size of the tip is well known, the number of atoms that contribute to the contact area may be less than might be inferred from the tip radius. In addition, if the tip contains irregularities (i.e. not perfectly smooth), these areas of the tip may contribute significantly to the interactions between the tip and the sample while only being a small geometric feature.

## Acknowledgments

MTK, PTM and JAH acknowledge support from ONR under contract N00014-09-WR20155. MTK and JAH also acknowledge partial support from AFOSR under contract F1ATA09086G002 and as part of the Extreme Friction MURI (F1ATA09086G001).

## References

- [1] Goddard W A, Brenner D W, Lyshevski S E and Iafrate G J (ed) 2007 *Handbook of Nanoscience, Engineering and Technology* (Boca Raton, FL: CRC Press LLC)
- [2] Krim J 1996 Friction at the atomic scale *Sci. Am.* **275** 74–80
- [3] Szlufarska I, Chandross M and Carpick R W 2008 Recent advances in single-asperity nanotribology *J. Phys. D: Appl. Phys.* **41** 123001
- [4] Dickson F 2006 An industry in transition: 2006 mems forecast *MEMS Industry Group, 2006*
- [5] Maboudian R, Ashurst W R and Carraro C 2002 Tribological challenges in micromechanical systems *Tribol. Lett.* **12** 95–100
- [6] Smallwood S A, Eapen K C, Patton S T and Zabinski J S 2006 Performance results of mems coated with a conformal DLC *Wear* **260** 1179–89
- [7] Gardos M N 1998 Advantages and limitations of silicon as a bearing material for mems applications *Tribology Issues and Opportunities in MEMS* ed B Bhushan (Boston, MA: Kluwer) pp 341–66
- [8] de Boer M P and Mayer T M 2001 Tribology of MEMS *Mater. Res. Soc. Bull.* **26** 302–4

- [9] Houston M R, Howe R T, Komvopoulos K and Maboudian R 1995 Diamond-like carbon films for silicon passivation in microelectromechanical devices *Mater. Res. Soc. Proc.* vol 383 pp 391–402
- [10] Maboudian R and Howe R T 1997 Review: adhesion in surface micromechanical structures *J. Vac. Sci. Technol. B* **15** 1–20
- [11] van Spengen W M 2003 MEMS reliability from a failure mechanisms perspective *Microelectron. Reliab.* **43** 1049–60
- [12] Zhao Y P, Wang L S and Yu T X 2003 Mechanics of adhesion in MEMS—a review *J. Adhes. Sci. Technol.* **17** 519–46
- [13] Srinivasan U, Houston M R, Howe R T and Maboudian R 1998 Alkyltrichlorosilane-based self-assembled monolayer films for stiction reduction in silicon micromachines *J. Microelectromech. Syst.* **7** 252–60
- [14] Sullivan J P, Friedmann T A and Hjort K 2001 Diamond and amorphous carbon MEMS *MRS Bull.* **26** 309–11
- [15] Webster J R, Dyck C W, Sullivan J P, Friedmann T A and Carton A 2004 Performance of amorphous diamond rf MEMS capacitive switch *Electron. Lett.* **40** 43–53
- [16] Auicello O, Birrell J, Carlisle J A, Gerbi J E, Xiao X C, Peng B and Espinosa H D 2004 Materials science and fabrication processes for a new mems technology based on ultrananocrystalline diamond thin films *J. Phys.: Condens. Matter* **16** R539–52
- [17] Love J C, Estroff L A, Kriebel J K, Nuzzo R G and Whitesides G M 2005 Self-assembled monolayers of thiolates on metals as a form of nanotechnology *Chem. Rev.* **105** 1103–69
- [18] Ulman A 1996 Formation and structure of self-assembled monolayers *Chem. Rev.* **96** 1533–54
- [19] Carpick R W and Salmeron M 1997 Scratching the surface: Fundamental investigations of tribology with atomic force microscopy *Chem. Rev.* **97** 1163–94
- [20] Salmeron M 2001 Generation of defects in model lubricant monolayers and their contribution to energy dissipation in friction *Tribol. Lett.* **10** 69–79
- [21] Lio A, Charych D H and Salmeron M 1997 Comparative atomic force microscopy study of the chain length dependence of frictional properties of alkanethiols *J. Phys. Chem. B* **101** 3800–5
- [22] van der Vegte E W, Subbotin A, Hadziioannou G, Ashton P R and Preece J A 2000 Nanotribological properties of unsymmetrical n-dialkyl sulfide monolayers on gold: effect of chain length on adhesion, friction, and imaging *Langmuir* **16** 3249–56
- [23] Lee S, Shon Y S, Colorado R, Guenard R L, Lee T R and Perry S S 2000 The influence of packing densities and surface order on the frictional properties of alkanethiol self-assembled monolayers (sams) on gold: a comparison of sams derived from normal and spiroalkanedithiols *Langmuir* **16** 2220–4
- [24] Li S, Cao P, Colorado R Jr, Yan X, Wenzl I, Shmakova O E, Graupe M, Lee T R and Perry S S 2005 Local packing environment strongly influences the frictional properties of mixed CH<sub>3</sub>- and CF<sub>3</sub>-terminated alkanethiol sams on Au(1 1 1) *Langmuir* **21** 933–6
- [25] Houston J E, Doelling C M, Vanderlick T K, Hu Y, Scoles G, Wenzl I and Lee T R 2005 Comparative study of the adhesion, friction, and mechanical properties of CF<sub>3</sub>- and CH<sub>3</sub>-terminated alkanethiol monolayers *Langmuir* **21** 3926–32
- [26] Kim H I, Graupe M, Oloba T, Doini O, Imaduddin S, Lee T R and Perry S S 1999 Molecularly specific studies of the frictional properties of monolayer films: a systematic comparison of CF<sub>3</sub>-, (CH<sub>3</sub>)<sub>2</sub>CH-, and CH<sub>3</sub>-terminated films *Langmuir* **15** 3179–85
- [27] Wong S S, Takano H and Porter M D 1998 Mapping orientation differences of terminal functional groups by friction force microscopy *Anal. Chem.* **70** 5209–12
- [28] Okabe Y, Akiba U and Fujihira M 2000 Chemical force microscopy of -CH<sub>3</sub> and -COOH terminal groups in mixed self-assembled monolayers by pulsed-force-mode atomic force microscopy *Appl. Surf. Sci.* **157** 398–404
- [29] Barrena E, Ocal C and Salmeron M 2001 A comparative afm study of the structural and frictional properties of mixed and single component films of alkanethiols on Au(1 1 1) *Surf. Sci.* **482-485** 1216–21
- [30] Brewer N M and Leggett G J 2004 Chemical force microscopy of mixed self-assembled monolayers of alkanethiols on gold: evidence for phase separation *Langmuir* **20** 4109–15
- [31] Lio A, Morant C, Ogletree D F and Salmeron M 1997 Atomic force microscopy study of the pressure-dependent structural and frictional properties of n-alkanethiols on gold *J. Phys. Chem. B* **101** 4767–73
- [32] Barrena E, Kopta S, Ogletree D F, Charych D H and Salmeron M 1999 Relationship between friction and molecular structure: alkylsilane lubricant films under pressure *Phys. Rev. Lett.* **82** 2880–3
- [33] Clear S C and Nealey P F 2001 Lateral force microscopy study of the frictional behavior of self-assembled monolayers of octadecyltrichlorosilane on silicon/silicon dioxide immersed in n-alcohols *Langmuir* **17** 720–32
- [34] Xiao X, Hu J, Charych D H and Salmeron M 1996 Chain length dependence of the frictional properties of alkylsilane molecules self-assembled on mica studied by atomic force microscopy *Langmuir* **12** 235–7

- [35] Brukman M J, Marco G O, Dunbar T D, Boardman L D and Carpick R W 2006 Nanotribological properties of alkanephosphonic acid self-assembled monolayers on aluminum oxide: effects of fluorination and substrate crystallinity *Langmuir* **22** 3988–98
- [36] Flater E E, Ashurst W R and Carpick R W 2007 Nanotribology of octadecyltrichlorosilane monolayers and silicon: self-mated versus unmated interfaces and local packing density effects *Langmuir* **23** 9242–52
- [37] Enachescu M, van den Oetelaar R J A, Carpick R W, Ogletree D F, Flipse C F J and Salmeron M 1998 Atomic force microscopy study of an ideally hard contact: the diamond(1 1 1) tungsten carbide interface *Phys. Rev. Lett.* **81** 1877
- [38] Carpick R W, Ogletree D F and Salmeron M 1999 A general equation for fitting contact area and friction vs load measurements *J. Colloid Interface Sci.* **211** 395
- [39] Luan B Q and Robbins M O 2005 The breakdown of continuum models for mechanical contacts *Nature* **435** 929
- [40] Luan B Q and Robbins M O 2006 Contact of single asperities with varying adhesion: comparing continuum mechanics to atomistic simulations *Phys. Rev. E* **74** 026111
- [41] Gao G, Cannara R J, Carpick R W and Harrison J A 2007 Atomic-scale friction on diamond: a comparison of different sliding directions on (0 0 1) and (1 1 1) surfaces using MD and AFM *Langmuir* **23** 5394–405
- [42] Pearson J D, Gao G, Zikry M A and Harrison J A 2009 Nanoindentation of model diamond nanocomposites: hierarchical molecular dynamics and finite-element simulations *Comput. Mater. Sci.* **47** 1–11
- [43] Lantz M A, O’Shea S J and Welland M E 1997 Simultaneous force and conduction measurements in atomic force microscopy *Phys. Rev. B* **56** 15345–52
- [44] Schwarz U D, Zworner O, Koster P and Wiesendanger R 1997 Quantitative analysis of the frictional properties of solid materials at low loads: I. Carbon compounds *Phys. Rev. B* **56** 6987
- [45] Kiely J D and Houston J E 1998 Nanomechanical properties of Au (1 1 1), (0 0 1), and (1 1 0) surfaces *Phys. Rev. B* **57** 12588–94
- [46] Enachescu M, van den Oetelaar R J A, Carpick R W, Ogletree D F, Flipse C F J and Salmeron M 1999 Observation of proportionality between friction and contact area at the nanometer scale *Tribol. Lett.* **7** 73–8
- [47] Riedo E, Chevrier J, Comin F and Brune H 2001 Nanotribology of carbon based thin films: the influence of film structure and surface morphology *Surf. Sci.* **477** 25–34
- [48] Socoliuc A, Bennewitz R, Gnecco E and Meyer E 2004 Transition from stick-slip to continuous sliding in atomic friction: entering a new regime of ultralow friction *Phys. Rev. Lett.* **92** 134301
- [49] Ritter C, Heyde M, Stegemann B, Rademann K and Schwarz U D 2005 Contact-area dependence of frictional forces: moving adsorbed antimony nanoparticles *Phys. Rev. B* **71** 085405
- [50] Bhushan B, Israelachvili J N and Landman U 1995 Nanotribology - friction, wear and lubrication at the atomic-scale *Nature* **374** 607–16
- [51] Brukman M J, Gao G, Nemanich R J and Harrison J A 2008 Temperature dependence of single-asperity diamond-diamond friction elucidated using afm and md simulations *J. Phys. Chem. C* **112** 9358–69
- [52] Johnson K L and Sridhar I 2001 Adhesion between a spherical indenter and an elastic solid with a compliant elastic coating *J. Phys. D: Appl. Phys.* **34** 683–9
- [53] Ebenstein D M and Wahl K J 2006 A comparison of JKR-based methods to analyze quasi-static and dynamic indentation force curves *J. Colloid Interface Sci.* **298** 652–62
- [54] Lin Y-Y, Chang C-F and Lee W-T 2008 Effects of thickness on the largely-deformed JKR (Johnson-Kendall-Roberts) test of soft elastic layers *Int. J. Solids Struct.* **45** 2220–32
- [55] Reedy E D 2006 Thin-coating contact mechanics with adhesion *J. Mater. Res.* **21** 2660–8
- [56] Rutland M W, Tyrrell J W G and Attard P 2004 Analysis of atomic force microscopy data for deformable materials *J. Adhes. Sci. Technol.* **18** 1199–215
- [57] Attard P 2002 Friction, adhesion, and deformation: dynamic measurements with the atomic force microscope *J. Adhes. Sci. Technol.* **16** 753–91
- [58] Plunkett M A and Rutland M W 2002 Dynamic adhesion of grafted polymer surfaces as studied by surface force measurements *J. Adhes. Sci. Technol.* **16** 983–96
- [59] Landman U, Luedtke W D, Burnham N A and Colton R J 1990 Atomistic mechanisms and dynamics of adhesion, nanoindentation, and fracture *Science* **248** 454–61
- [60] Hoover W G, Degroot A J, Hoover C G, Stowers I F, Kawai T, Holian B L, Boku T, Ihara J and Belak S 1990 Large-scale elastic–plastic indentation simulations via nonequilibrium molecular-dynamics *Phys. Rev. A* **42** 5844–53
- [61] Tomagnini O, Ercolessi F and Tosatti E 1993 Microscopic interaction between a gold tip and a Pb(1 1 0) surface *Surf. Sci.* **287–288** 1041–5
- [62] Harrison J A, White C T, Colton R J and Brenner D W 1992 Nanoscale investigation of indentation, adhesion, and fracture of diamond (1 1 1) surfaces *Surf. Sci.* **271** 57–67

- [63] Harrison J A, Stuart S J, Robertson D H and White C T 1997 Properties of capped nanotubes when used as spm tips *J. Phys. Chem. B* **101** 9682–5
- [64] Tutein A B, Stuart S J and Harrison J A 1999 Indentation analysis of linear-chain hydrocarbon monolayers anchored to diamond *J. Phys. Chem. B* **103** 11357–65
- [65] Wolf D, Yamakov V, Phillpot S R, Mukherjee A and Gleiter H 2005 Deformation of nanocrystalline materials by molecular-dynamics simulation: relationship to experiments? *Acta Mater.* **53** 1–40
- [66] Van Swygenhoven J R and Weertman H 2006 Deformation in nanocrystalline metals *Mater. Today* **9** 24–31
- [67] Schall J D, Mikulski P T, Chateauneuf G M, Gao G T and Harrison J A 2007 Molecular dynamics simulations of tribology *Superlubricity* ed A Erdemir and J-M Martin (Amsterdam: Elsevier) pp 79–102
- [68] Szlufarska I, Kalia R K, Nakano A and Vashishta P 2007 A molecular dynamics study of nanoindentation of amorphous silicon carbide *J. Appl. Phys.* **102** 023509
- [69] Gouldstone A, Chollacoop N, Dao M, Li J, Minor A M and Shen Y L 2007 Indentation across size scales and disciplines: recent developments in experimentation and modeling *Acta Mater.* **55** 4015–39
- [70] Knippenberg M T, Mikulski P T, Dunlap B I and Harrison J A 2008 Atomic contributions to friction and load for tip-self assembled monolayer interactions *Phys. Rev. B* **78** 235409
- [71] Harrison J A, White C T, Colton R J and Brenner D W 1992 Molecular-dynamics simulations of atomic-scale friction of diamond surfaces *Phys. Rev. B* **46** 9700–8
- [72] Harrison J A, Stuart S J and Brenner D W 1999 Atomic-scale simulation of tribological and related phenomena *Handbook of Micro/Nanotribology* 2nd edn ed B Bhushan (Boca Raton, FL: CRC Press) pp 525–94
- [73] Robbins M O and Müser M H 2001 Computer simulations of friction, lubrication, and wear *Modern Tribology Handbook* ed B Bhushan vol I (Boca Raton, FL: CRC Press) pp 717–71
- [74] Gao G T, Mikulski P T and Harrison J A 2002 Molecular-scale tribology of amorphous carbon coatings: effects of film thickness, adhesion, and long-range interactions *J. Am. Chem. Soc.* **124** 7202–9
- [75] Harrison J A, Gao G T, Harrison R J, Chateauneuf G M and Mikulski P T 2004 The friction of model self-assembled monolayers *Encyclopedia of Nanoscience and Nanotechnology* ed H S Nalwa vol 3 (Los Angeles, CA: American Scientific Publishers) pp 511–27
- [76] Heo S J, Sinnott S B, Brenner D W and Harrison J A 2005 Computational modeling of nanometer-scale tribology *Nanotribology and Nanomechanics: An Introduction* ed B Bhushan (Heidelberg: Springer) pp 623–91
- [77] Mikulski P T and Harrison J A 2001 Packing-density effects on the friction of *n*-alkane monolayers *J. Am. Chem. Soc.* **123** 6873–81
- [78] Sung I H and Kim D E 2005 Molecular dynamics simulation study of the nano-wear characteristics of alkanethiol self-assembled monolayers *Appl. Phys. A—Mater. Sci. Proc.* **81** 109–14
- [79] Chandross M, Lorenz C D, Stevens M J and Grest G S 2008 Simulations of nanotribology with realistic probe tip models *Langmuir* **24** 1240–6
- [80] Mo Y, Turner K T and Szlufarska I 2009 Friction laws at the nanoscale *Nature* **457** 1116–9
- [81] Mikulski P T, Gao G, Chateauneuf G M and Harrison J A 2005 Contact forces at the sliding interface: mixed versus pure model alkane monolayers *J. Chem. Phys.* **122** 024701
- [82] Mikulski P T, Herman L A and Harrison J A 2005 Odd and even model self-assembled monolayers: links between friction and structure *Langmuir* **21** 12197–206
- [83] Harrison J A, Schall J D, Knippenberg M T, Gao G T and Mikulski P T 2008 Elucidating atomic-scale friction using md and specialized analysis techniques *J. Phys.: Condens. Matter* **20** 354009
- [84] Stuart S J, Tutein A B and Harrison J A 2000 A reactive potential for hydrocarbons with intermolecular interactions *J. Chem. Phys.* **112** 6472–86
- [85] Delcorte A, Bertrand P and Garrison B J 2001 Collision cascade and sputtering process in a polymer *J. Phys. Chem. B* **105** 9474–86
- [86] Marian J, Zepeda-Ruiz L A, Gilmer G H, Bringa E M and Rognlien T 2006 Simulations of carbon sputtering in amorphous hydrogenated samples *Phys. Scr.* **T124** 65–9
- [87] Smiley E J, Postawa Z, Wojciechowski I A, Winograd N and Garrison B J 2006 Coarse-grained molecular dynamics studies of cluster-bombarded benzene crystals *Appl. Surf. Sci.* **252** 6436–9
- [88] Ni B, Sinnott S B, Mikulski P T and Harrison J A 2002 Compression of carbon nanotubes filled with C<sub>60</sub>, CH<sub>4</sub>, or Ne: predictions from molecular dynamics simulations *Phys. Rev. Lett.* **88** 205505-1–205505-4
- [89] Knippenberg M T, Stuart S J, Cooper A C, Pez G P and Cheng H S 2006 Physical adsorption strength in open systems *J. Phys. Chem. B* **110** 22957–60
- [90] Wang Z, Devel M, Langlet R and Dulmet B 2007 Electrostatic deflections of cantilevered semiconducting single-walled carbon nanotubes *Phys. Rev. B* **75** 205414
- [91] Grujicic M, Cao G and Roy W N 2005 Computational analysis of the lattice contribution to thermal conductivity of single-walled carbon nanotubes *J. Mater. Sci.* **40** 1943–52

- [92] Harrison J A and Brenner D W 1994 Simulated tribochemistry: an atomic-scale view of the wear of diamond *J. Am. Chem. Soc.* **116** 10399–402
- [93] Fenter P, Eberhardt A and Eisenberger P 1994 Self-assembly of *n*-alkyl thiols as disulfides on Au(1 1 1) *Science* **266** 1216
- [94] Berendsen H J C, Postma J P M, van Gunsteren W F, DiNola A and Haak J R 1984 Molecular dynamics with coupling to an external bath *J. Chem. Phys.* **81** 3684–90
- [95] Perry M D and Harrison J A 1995 Universal aspects of the atomic-scale friction of diamond surfaces *J. Phys. Chem.* **99** 9960–5
- [96] Chandross M, Grest G S and Stevens M J 2002 Friction between alkylsilane monolayers: molecular simulation of ordered monolayers *Langmuir* **18** 8392–9
- [97] Park B, Chandross M, Stevens M J and Grest G S 2003 Chemical effects on the adhesion and friction between alkanethiol monolayers: molecular dynamics simulations *Langmuir* **19** 9239–45
- [98] Dunlap B I and Zope R R 2006 Efficient quantum-chemical geometry optimization and the structure of large icosahedral fullerenes *Chem. Phys. Lett.* **422** 451–4
- [99] Harrison J A, Gao G T, Schall J T, Knippenberg M T and Mikulski P T 2008 Friction between solids *Phil. Trans. R. Soc. A* **366** 1469–95
- [100] Chandross M, Webb III E B, Stevens M J, Grest G S and Garafalini S H 2004 Systematic study of the effect of disorder on nanotribology of self-assembled monolayers *Phys. Rev. Lett.* **93** 166103
- [101] Mikulski P T and Harrison J A 2001 Periodicities in the properties associated with the friction of model self-assembled monolayers *Tribol. Lett.* **10** 29–38
- [102] Mikulski P T, Chateaufneuf G M, Knippenberg M T, Van Workum K and Harrison J A 2010 *J. Chem. Phys.* submitted
- [103] Tutein A B, Stuart S J and Harrison J A 2000 Role of defects in the compression and friction of anchored hydrocarbon chains on diamond *Langmuir* **16** 291–6
- [104] Johnson K L 1985 *Contact Mechanics* (Cambridge: Cambridge University Press)
- [105] Derjaguin B V, Muller V M and Toporov Y P 1975 Effect of contact deformations on adhesion of particles *J. Colloid Interface Sci.* **53** 314
- [106] Johnson K L, Kendall K and Roberts A D 1971 Surface energy and contact of elastic solids *Proc. R. Soc. Lond. A* **324** 301
- [107] Piotrowski P L, Cannara R J, Gao G, Urban J J, Carpick R W and Harrison J A Atomistic factors governing adhesion between diamond, amorphous carbon, and model diamond nanocomposite surfaces *J. Adhes. Sci. Technol.* at press
- [108] DelRio F W, Jaye C, Fischer D A and Cook R F 2009 Elastic and adhesive properties of alkanethiol self-assembled monolayers on gold *Appl. Phys. Lett.* **94** 131909
- [109] Salmeron M, Neubauer G, Folch A, Tomitori M, Ogletree D F and Sautet P 1993 Viscoelastic and electrical-properties of self-assembled monolayers on Au(1 1 1) films *Langmuir* **9** 3600–11
- [110] Henda R, Grunze M and Pertsin A J 1998 Static energy calculations of stress–strain behavior of self-assembled monolayers *Tribol. Lett.* **5** 191–5
- [111] Burns A R, Houston J E, Carpick R W and Michalske T A 1999 Friction and molecular deformation in the tensile regime *Phys. Rev. Lett.* **82** 1181–4
- [112] Oncins G, Vericat C and Sanz F 2008 Mechanical properties of alkanethiol monolayers studied by force spectroscopy *J. Chem. Phys.* **128** 044701
- [113] Engelkes V B and Frisbie C D 2006 Simultaneous nanoindentation and electron tunneling through alkanethiol self-assembled monolayers *J. Phys. Chem. B* **110** 10011–20
- [114] Brewer N M, Beake B D and Leggett G J 2001 Friction force microscopy of self-assembled monolayers: influence of adsorbate alkyl chain length, terminal group chemistry, and scan velocity *Langmuir* **17** 1970–4
- [115] Wong S S, Joselevich E, Woolley A T, Cheung C L and Lieber C M 1998 Covalently functionalized nanotubes as nanometre-sized probes in chemistry and biology *Nature* **394** 52–5